AN EXAMPLE OF MOLD COMPENSATION BY MEANS OF NUMERICAL SIMULATION ON A GENERIC CURVED CFRP C-SPAR

B. Wucher[1*], F. Lani[2], P. Martiny[1], T. Pardoen[2], C. Bailly[3]

[1]*Composites Structures and Processes, Cenaero, Rue des Frères Wright 29 6041 Gosselies Belgium*
[2]*Institute of Mechanics, Materials and Civil Engineering, Université catholique de Louvain, Place Sainte Barbe 2, 1348 Louvain-la-Neuve, Belgium*
[3]*Institute of Condensed Matter and Nanosciences, Université catholique de Louvain, Croix du Sud 1, 1349 Louvain-la-Neuve, Belgium*
**benoit.wucher@cenaero.be*

Keywords: mold compensation, curing, numerical simulation.

Abstract
Manufacturing a composite part with a well-defined shape is challenging due to the distortions during the curing process. A computationally-driven mold compensation strategy is proposed in this paper, based on an in-house surrogate-based optimizer and on 3D curing simulations. A parametrization and post-treatment approach are proposed and tested on a generic curved CFRP C-spar geometry.

1 Introduction

Typical epoxy-based composite materials show significant distortions as a consequence of the manufacturing process. These distortions lead to deviations with respect to the manufacturing tolerances and to assembling difficulties. The physical origin for the distortion is a combination of several phenomena, of which the most important are the chemical shrinkage, the mismatch of coefficient of thermal expansion (CTE) between the fibers and the matrix, and the partly irreversible thermal expansion of the resin due to the significant CTE variations during the cure. Cure-induced distortions are most commonly observed as spring-in or warpage of the composite part after removal from the mold.

Two main approaches can be investigated to reduce the discrepancy between the nominal geometry and the final part. A first option is to improve the manufacturing process. Teoh and Hsiao [1] observed a spring-in reduction of L-shaped parts by using the multistage curing technique and the Vacuum Assisted Resin Transfer Molding (VARTM) process. Hsiao and Gangireddy [2] proposed to include carbon nanofibers in a polyester resin to reduce the anisotropy of the thermal expansion of the material and, hence, reduce the spring-in. Both of these methods increase drastically the complexity of the manufacturing process. Jain et al. [3] optimized experimentally the spring-in of a thermoplastic C-shaped aileron rib by changing the cure temperature. A second option consists in altering the shape of the mold so that the final part is as close as possible to the nominal geometry. This approach is called mold compensation, and is the subject of the present work. Dong [4] developed a simplified curing model, created designs of experiments for several basic composite structures with only a few parameters and developed a regression-based spring-in reduction method. Dong [5] studied the effect of the curing process on a parametrized stiffener structure but did not include the

model in an optimization loop. Zhu and Geubelle [6] used an optimizer to compensate the mold shape for L-shaped parts.

All these methods have been tested only on L-shaped-like composite parts, and therefore do not provide a systematic distortion compensation for complex geometries. This paper presents an attempt to fill this gap. A full optimization chain is developed, including CAD parametrization, automatic draping simulation and a 3D computationally-efficient chemical-mechanical curing model. This chain is then used in an in-house surrogate-based optimizer called MINAMO [7] to modify the geometry of the mold and to minimize the mismatch between the nominal and actual shape of the part after demolding. The combination of automatic draping and surrogate models allows to imagine the application of this technique to virtually any geometry. A moderately complex geometry is tested in this work, namely a stiffened curved CFRP C-spar. Individual optimizations are performed for each parameter and show their inadequacy, emphasizing the need for a surrogate-based optimization on the entire structure. The paper is organized as follows. First, the test case geometry is introduced. Then, the different components of the optimization chain, such as draping and curing simulation, are developed. Finally, the optimization strategy itself and the results obtained are presented.

2 Test case

2.1 Geometry

The chosen test case is a generic stiffened curved C-spar, as shown in Fig. 1. It was modeled as a surface because it is easier to create the CAD model and much easier to drape compared to a volume model. This geometry was selected because it is simple enough to anticipate its cure-induced distortion behavior, and complex enough to enforce the need for a draping simulation, in particular because of the stiffeners. The dimensions are 800 mm in curvilinear length, 100 mm in width and 50 mm in height. The fillet radius along the length of the C-spar and at the stiffeners is 6 mm. The C-spar is curved and forms an arc of a circle with a radius of 1500 mm.

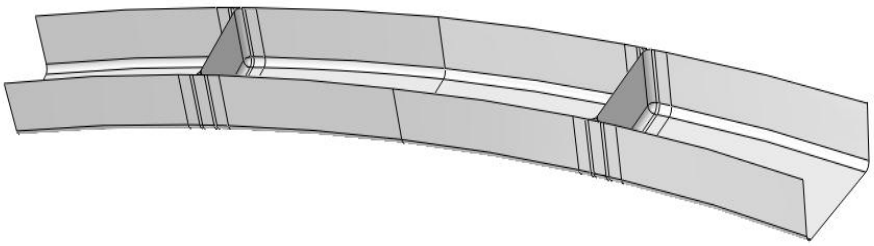

Figure 1. Surface geometry of the curved C-spar.

2.2 Material

For this proof of concept, the material properties of a common carbon/epoxy resin system were selected, namely the 8552/AS4. The degree of cure at gelation is equal to 0.31 [8]. The mechanical properties are listed in Table 1 and are taken from [8,9]. The relationships between the degree of cure *X* and the glass transition temperature, the kinetic model and the transverse chemical shrinkage model are given by Eq. 1, Eq. 2 and Eq. 3, respectively [8], with *T* being the temperature in Kelvin and *R* being the universal gas constant. Chemical shrinkage in the fiber direction is assumed to be null.

$$T_g\ (°C) = 164.6\,X^2 + 51\,X + 2.67 \tag{1}$$

Property	Rubbery state (average values)	Glassy state (average values)
E_L	131.000 MPa	133.000 MPa
E_T	122 MPa	9.130 MPa
ν_{LT}	0.33	0.28
ν_T	0.64	0.47
G_{LT}	41.1 MPa	5.210 MPa
G_T	37.2 MPa	3.210 MPa
α_L (CTE)	0 /°C	0 /°C
α_T (CTE)	2.10^{-4} /°C	$3.26.10^{-5}$ /°C

Table 1. Mechanical properties of 8552/AS4 system during cure [8,9]. Subscript *L* strands for fiber direction, *T* stands for transverse direction. α is the coefficient of thermal expansion (CTE).

$$\frac{dX}{dt}\ (s^{-1}) = \frac{7.10^4\ e^{-6.5.10^4/RT}\ X^{0.5}\ (1-X)^{1.5}}{1+\ e^{30(X+1.5148-5.171.10^{-3}T)}} \tag{2}$$

$$\varepsilon_{ch}(\%) = 2.16\ X^3 - 1.62\ X^2 - 2.7\ X + 0.93 \tag{3}$$

3 Components of the computational chain

3.1 Draping

The draping simulation is performed with Simulayt [10] on the surface geometry. The seed point is taken in the middle of the part, so that the draping is as balanced as possible. A seed curve is introduced to follow the longitudinal curvature of the spar. The result is shown in Fig 2. A $[0_2, 90_2]_S$ layup is used for the C-spar itself, and the stiffeners are made up of four zero-degree plies.

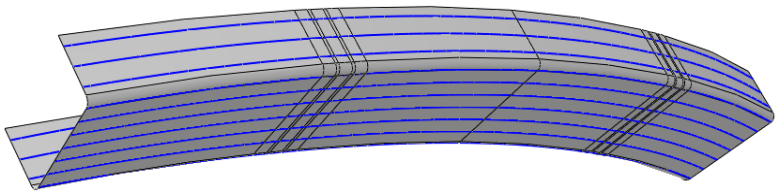

Figure 2. Draping simulation of a 0° ply on the C-spar.

3.2 Extrusion

The output of the draping simulation is a shell model, on which a curing simulation cannot be performed without an adapted constitutive model. Indeed, the through-thickness behavior needs to be taken into account because, as stated earlier, the main cause for spring-in is the mismatch between the through-thickness and in-plane CTEs. Hence, a volume model must be obtained from the draped surface. This is performed by an in-house tool, which extrudes the surface mesh and creates hexahedral elements 0.2 mm in thickness [11] for each ply, with the right orientation. The resulting mesh has one element per ply in the thickness direction and contains a total of 450.000 degrees of freedom.

3.3 Curing model

Since the curing simulations are included within an optimization loop, they should be as computationally efficient as possible. For this reason, we assume that the temperature is uniform throughout the part. This is a valid hypothesis (the C-spar is 0.8 mm thick and 800 mm long), and it limits the analysis to a mechanical-chemical problem only, instead of a transient coupled thermo-mechanical-chemical one.

The mechanical model used in this study for the curing is the one developed by Svanberg and Holmberg [12]. The main assumptions include the fact that no stresses build up before the gel point, and the material properties are constant within each state of the material (rubbery or glassy). Since no stresses build up before gelation, the simulation starts with an initial degree of cure of 0.31. The part is then cured for 8.500 seconds, including 1.000 seconds for cool-down. The time step is set equal to 100 seconds, which is small enough to capture the correct evolution of the degree of cure, and large enough to enable an efficient computation time. Free boundary conditions are used, i.e. only rigid body modes are suppressed and the mold itself is not modeled. The validity of this assumption largely depends on the actual manufacturing process, particularly the friction between the composite part and the mold can play a role. However, in this work, we do not focus on the accuracy of the curing model, but on the mold compensation technique.

The duration of the curing simulation on the C-spar (450.000 degrees of freedom) is equal to 15 minutes on six cores of a double hexa-core Intel Xeon (3.07 GHz) computation node. This duration is quite satisfactory, considering that this is a transient simulation and a relatively large model. The analysis necessitates about 6 GB of RAM per core and is performed with Abaqus/Standard [13] through a user material (UMAT) for the implementation of the constitutive law.

4 Parametrization and post-processing

In order to have an efficient parametrization, the cure-induced deformation modes must be assessed. The result of the curing simulation is shown in Fig. 3 and the observed deformation modes are explained in Fig. 4. As expected, spring-in develops in the sections that are not held in place by a stiffener. Moreover, the radius of curvature of the C-spar decreases and some torsion appears.

The proposed parametrization is meant to compensate for these distortions (Fig. 5). The walls of the C-spar are bent outwards to compensate the spring-in. The angles θ_k and β_k are introduced in section k (k = 1,2,3) to control the outer and inner angles of each section. The radius of curvature of the part is increased slightly by controlling the parameter $d = D1 - D2$ (see Fig. 6). The torsion is induced by the angle φ in the opposite direction to the one caused by the curing, so that the C-spar can be horizontal after cure. The curvature change and torsion are distributed progressively along the length of the C-spar. Each angle and length is parametrized separately, and the symbols representing these parameters are recalled in Table 2.

The parametrization is made up of 8 parameters: six spring-in angles, one torsion angle, one curvature change. Each parameter corresponds to one observed mode of distortion. These phenomena have to be measured in order to compute the discrepancy between the cured part and the target geometry. For this purpose, the curing simulation is post-processed as follows:

- each spring-in angle S_{ik} (inner angle) and S_{ok} (outer angle) is computed on the cured part,
- the curvature change is evaluated as the difference $D = D2 - D3$ (Fig. 6),
- the torsion is evaluated by the angle H between the bottom line of Section number 3 and the horizontal plane.

All these results are transformed into adimensional terms by dividing them by their initial value obtained from the uncompensated cured part. The cost function of the optimization consists of reducing the sum of all these adimensional values (see Eq. 4). Thus, the optimization is mono-objective.

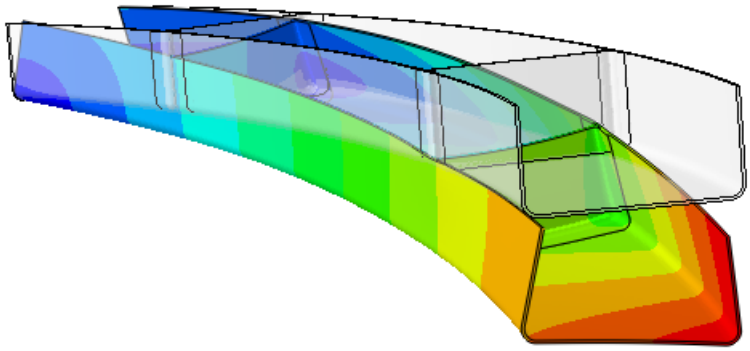

Figure 3. Displacement card after cure and comparison to nominal geometry (deformation factor : 5). Torsion and spring-in can be clearly observed.

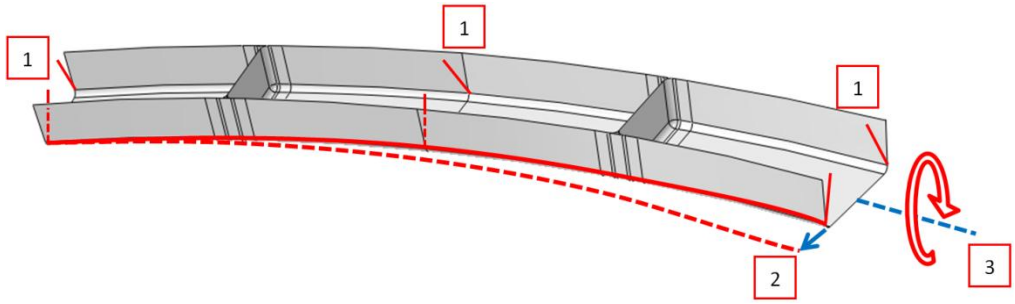

Figure 4. Deformation modes during cure. (1) Spring-in where there is no stiffener, (2) Global curvature of the C-spar decreases, (3) Torsion.

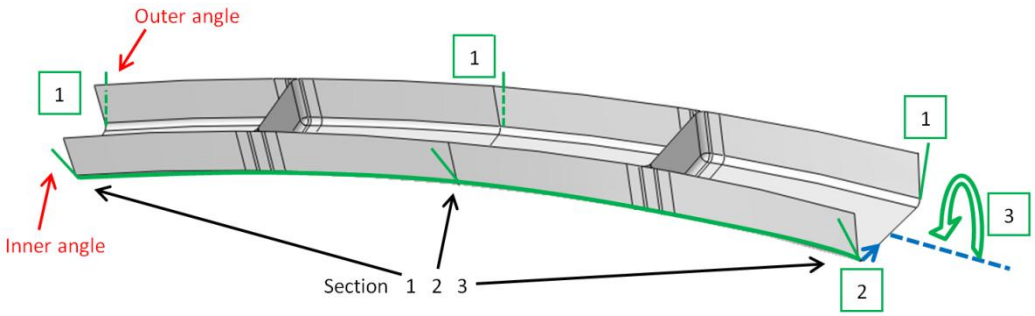

Figure 5. Compensated geometry. (1) Each section is opened to compensate spring-in, (2) The radius of curvature of the C-spar is increased, (3) The C-spar is twisted in the opposite direction to the cure-induced torsion.

Compensated phenomenon	**Symbol for compensation parameter**	**Symbol for post-processing value**
Spring-in in section k (inner angle)	θ_k	S_{ik}
Spring-in in section k (outer angle)	β_k	S_{ok}
Curvature change	$d = D1 - D2 > 0$ (Fig. 9)	$D = D2 - D3$ (Fig. 9)
Torsion	φ	H

Table 2. Notation for compensation parameters and their corresponding post-processing values.

To sum up, the optimization parameters are θ_k , β_k, (k = 1,2,3), d and φ, and the objective function is given by,

$$F_{obj} = \sum_{k=1}^{3}\left(\frac{S_{ik}}{S_{ik,0}} + \frac{S_{ok}}{S_{ok,0}}\right) + \frac{H}{H_{,0}} + \frac{D}{D_{,0}} \quad (4)$$

where the subscript ",0" means computed value from cured nominal geometry (Fig. 6).

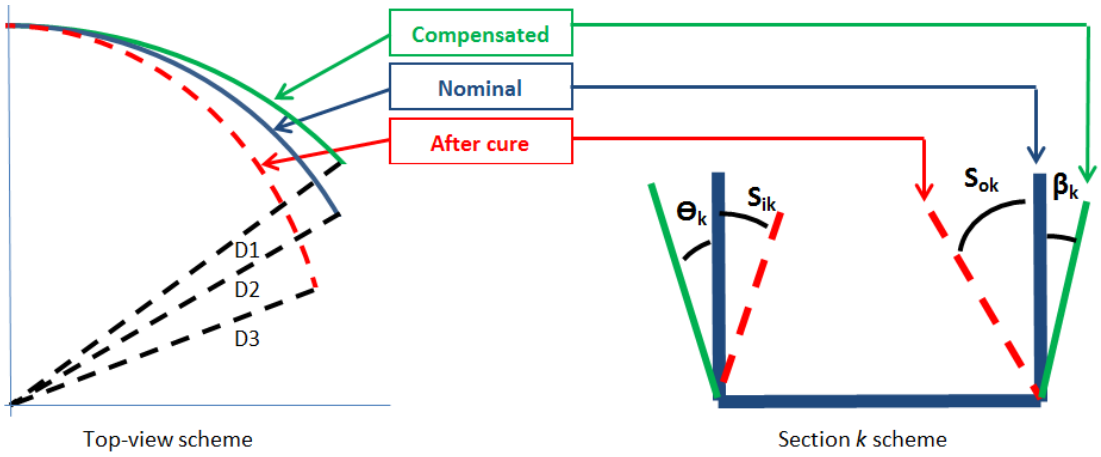

Figure 6. Left: Schematic (top-view of C-spar) explaining how the curvature change is parametrized and post-processed. Right: view of a cross-section and definition of the spring-in and compensation angles.

5 Optimization results

5.1 Individual optimizations

In a first approach, each parameter is optimized individually. That is, for each parameter, 20 experiments are computed with a different value of this particular parameter, while the other parameters are kept constant. Design of experiments are performed within a range of [0, 3°] for angles and [0, 5 mm] for *d*. Results are summed up in Table 3. Column 1 presents the initial values of each deformation mode. Column 2 lists the relative values of the deformation modes which have been individually optimized. Each deformation mode was reduced to a maximum of 2.2 % of its initial value, which is very satisfactory. The input parameters that correspond to these optima are given in Column 3. Then, a curing simulation is run using all the individually optimized parameters together, and the relative values of the deformation modes are given in Column 4. These last results emphasize the coupling between all the parameters. For example, a value of φ = 2.02° leads to H / $H_{,0}$ = 2.2 % when all the other parameters have their nominal value (i.e. 0° for angles and 0 mm for *d*), but the same value of φ leads to H / $H_{,0}$ = 140 % when all the optimized parameters are used. The fact that a coupling between the parameters exists makes individual optimizations irrelevant and enforces the use of an eight-parameter optimization to solve our mold compensation problem.

Moreover, whereas all spring-in angles are very easy to optimize thanks to a fairly linear behavior, it is not the case at all for the torsion deformation mode. Figure 7 shows that the spring-in angles are easily optimized individually, but the torsion shows a highly non-linear behavior. While pure genetic optimization could still be performed with such non-linearity if there is only one parameter, it becomes virtually impossible when there are eight parameters which are not uncoupled: it would require far too many curing simulations to reach the optimum.

These observations clearly justify the use in this study of a Surrogate-based optimization (SBO) strategy on the entire parametrized structure. Surrogate models are mathematical models approximating the full response surface based on the simulated design of experiment. Properly captured non linearities help the optimizer find the optimum with much fewer simulations compared to a classic genetic optimization. For more information, see [7].

Initial deformation value	**Relative deformation values which have been individually optimized**	**Optimal parameters corresponding to each optimum deformation**	**Results when all optimized parameters are used**
$S_{o1,0}$ = 2.69°	$S_{o1} / S_{o1,0}$ = 1 %	β_1 = 2.53°	$S_{o1} / S_{o1,0}$ = 15 %
$S_{o2,0}$ = 2.48°	$S_{o2} / S_{o2,0}$ = 0.08 %	β_2 = 2.10°	$S_{o2} / S_{o2,0}$ = 7 %
$S_{o3,0}$ = 2.28°	$S_{o3} / S_{o3,0}$ = 0.2 %	β_3 = 2.38°	$S_{o3} / S_{o3,0}$ = 4 %
$S_{i1,0}$ = 2.27°	$S_{i1} / S_{i1,0}$ = 0.6 %	θ_1 = 2.54°	$S_{i1} / S_{i1,0}$ = 13 %
$S_{i2,0}$ = 2.55°	$S_{i2} / S_{i2,0}$ = 1.6 %	θ_2 = 2.23°	$S_{i2} / S_{i2,0}$ = 5 %
$S_{i3,0}$ = 1.87°	$S_{i3} / S_{i3,0}$ = 0.1 %	θ_3 = 2.08°	$S_{i3} / S_{i3,0}$ = 12 %
$H_{,0}$ = 1.24°	$H / H_{,0}$ = 2.2 %	φ = 2.02°	$H / H_{,0}$ = 140 %
$D_{,0}$ = 1.1 mm	$D / D_{,0}$ = 1.8 %	d = 0.6 mm	$D / D_{,0}$ = 77 %

Table 3. Results of individual optimizations. Each deformation mode can be reduced individually, but the combination of all optimized parameters is not as efficient, especially for *H* and *D*.

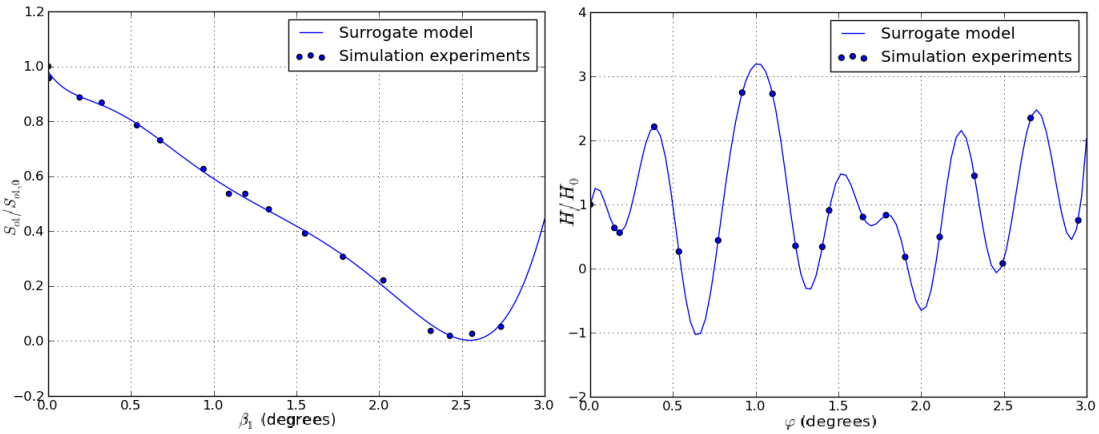

Figure 7. Left : variation of the relative deformation mode $S_{o1} / S_{o1,0}$ (outer spring-in in section 1) with respect to its driving angle parameter β_1.
Right : variation of the relative deformation mode $H / H_{,0}$ (torsion) with respect to its driving angle φ.

5.2 Eight-parameter optimization

The SBO was launched on the fully-parametrized C-spar. A design of experiments of 70 individuals was performed, after which the leave-one-out coefficient (indicator of the quality of the surrogate) for the objective function (Eq. 4) was 0.62, which is quite satisfactory. The optimization itself was then launched and the optimum was obtained after 34 iterations, that is 70 + 34 = 104 curing simulations or approximately 26 hours of total computational time on six processors. The optimum is presented in Table 4. The distortions could not be entirely suppressed since one spring-in angle is still at 20 % of its initial value (which means it was reduced by 80 %). However, this solution is better than the one obtained

with individual optimizations, where spring-in was slightly more reduced but torsion was increased. The eight-parameter optimization enabled us to find a more evenly improved specimen, and the average distortion left is 9.6 %. Therefore, the discrepancy between the cured part and the nominal geometry was reduced by about 90 %, which is a solid proof that the strategy developed in this work filled its purpose, which was to propose a computational mold compensation chain.

Absolute deformation values for the optimum individual	**Relative deformation values for the optimum individual**	**Optimal parameters**
S_{o1} = 0.38°	$S_{o1} / S_{o1,0}$ = 14 %	β_1 = 2.21°
S_{o2} = 0.07°	$S_{o2} / S_{o2,0}$ = 3 %	β_2 = 2.30°
S_{o3} = 0.30°	$S_{o3} / S_{o3,0}$ = 13 %	β_3 = 2.65°
S_{i1} = 0.18°	$S_{i1} / S_{i1,0}$ = 8 %	θ_1 = 2.5°
S_{i2} = 0.51°	$S_{i2} / S_{i2,0}$ = 20 %	θ_2 = 2.98°
S_{i3} = 0.11°	$S_{i3} / S_{i3,0}$ = 6 %	θ_3 = 2.29°
H = 0.1°	$H / H_{,0}$ = 0.6 %	φ = 1.63°
D = 0.1 mm	$D / D_{,0}$ = 12 %	d = 1.5 mm
	Average: 9.6 %	

Table 4. Optimum found by the eight-parameter optimization

6 Conclusion

A computational chain designed to compensate for cure-induced distortions was presented in this work. Several tools were developed to benefit from the high-fidelity draping on a surface model as well as from 3D curing simulations. A parametrization of the test-case geometry was proposed based on observed distortions of the nominal geometry, and the need for surrogate-based multi-parameter optimization in order to reduce those deformations was brought to light. However, the present approach is very geometry-dependent. In particular, the parametrization and post-processing that were used cannot be applied to another geometry. A systematic approach that would be valid on any kind of geometry without additional development was tested but resulted in a less efficient optimization. Further investigation has to be made in that direction.

References

[1] Teoh K.J., Hsiao K.T. Improved dimensional infidelity of curve-shaped VARTM composite laminates using a multi-stage curing technique – Experiments and modeling. *Composites : Part A*, **42**, pp. 762-771 (2011).

[2] Hsiao K.T., Gangireddy S. Investigation on the spring-in phenomenon of carbon nanofiber-glass fiber/polyester composites manufactured with vacuum assisted resin transfer molding. *Composites : Part A*, **39**, pp. 834-842 (2008).

[3] Jain L., Hou M., Ye L., Mai Y.W. Spring-in study of the aileron rib manufactured from advanced thermoplastic composite. *Composites : Part A*, **29A**, pp. 973-979 (1998).

[4] Dong C. Dimension variation prediction and control for composites. Thesis. Florida State University (2003).

[5] Dong C. Process-induced deformation of composite T-stiffener structures. *Composite Structures*, **92**, pp. 1614-1619 (2010).

[6] Zhu Q., Geubelle P. Dimensional accuracy of thermoset composites : shape optimization. *Journal of Composite Materials*, **36**, pp. 647-672 (2002).
[7] Sainvitu C., Iliopoulou V., Lepot I. Global optimization with expensive functions – sample turbomachinery design application. Recent Advances in Optimization and its Applications in Engineering, Springer, pp. 499-509 (2010).
[8] Ersoy N., Potter K., Winsom M.R., Clegg M.J. Development of spring-in angle during cure of a thermosetting composite. *Composites : Part A*, **36**, pp. 1700-1706 (2005).
[9] Ersoy N., Garstka T., Potter K., Winsom M.R., Porter D., Clegg M., Stringer G. Development of the properties of a carbon fibre reinforced thermosetting composite during cure. *Composites : Part A*, **41**, pp. 401-409 (2010).
[10] Simulayt software package, www.simulayt.com.
[11] Vargas G., Mujika F. Determination of in-plane shear properties by three-point flexure test of ±45° anti-symmetric laminates. *Polymer Testing*, **30**, pp. 204-215 (2011).
[12] Svanberg J.M., Holmberg J.A. Prediction of shape distorsions Part I. FE-implementation of a path dependent constitutive model. *Composites : Part A*, **35**, pp. 711-721 (2004).
[13] ABAQUS Standard Finite Element Package, Dassault Systèmes, www.abaqus.com.